Journal of Alloys and Compounds 509 (2011) 7034–7037

Contents lists available at ScienceDirect

Journal of Alloys and Compounds

journal homepage: www.elsevier.com/locate/jallcom

Electrochemical performance of multi-element doped α-nickel hydroxide prepared by supersonic co-precipitation method

Z.J. Zhang, Y.J. Zhu*, J. Bao, X.R. Lin, H.Z. Zheng

School of Physics and Optoelectronic Engineering, Guangdong University of Technology, Guangzhou 510006, China

ARTICLE INFO

Article history:
Received 17 December 2010
Received in revised form 17 March 2011
Accepted 17 March 2011
Available online 29 March 2011

Keywords:
Supersonic co-precipitation
Multi-element doped α-nickel hydroxides
Reaction reversibility
Proton diffusion coefficient

ABSTRACT

The multi-element doped α-nickel hydroxides have been prepared by supersonic co-precipitation method. Three kinds of samples A, B, C were prepared by chemically coprecipitating Ni, Al, Co, Y, Zn. It was found that sample C produced better performance than the others. The cyclic voltammetry (CV) and electrochemical impedance spectroscopy (EIS) measurements indicated that sample C has better electrochemical performance, such as better reaction reversibility, higher proton diffusion coefficient and lower charge-transfer resistance, than those of samples A and B. The charge–discharge tests showed that the discharge capacity (346 mA h/g) of sample C is even larger at 0.5 C rate than that (337mAh/g) at 0.1 C rate, while the discharge capacity at 0.5 C rate is much lower than that at 0.1 C rate for samples A and B. It indicates that all doped elements can produce the synergic effect and further improve the electrochemical properties of the active materials.

1. Introduction

As the positive material for Ni-MH batteries, nickel hydroxide has two phases known as α-$Ni(OH)_2$ and β-$Ni(OH)_2$. It is generally believed that α-$Ni(OH)_2$ shows superior electrochemical properties to β-$Ni(OH)_2$ with a much higher discharge capacity and no mechanical swelling deformation [1]. However, the α-$Ni(OH)_2$ is unstable in strong alkaline media and easily converted into β-$Ni(OH)_2$. To improve the stability of α-$Ni(OH)_2$, partial substitution of nickel ions by other metal ions, such as Al [2–4], Co [5], Fe [6], Zn [7], is commonly used method. Although a stable α phase structure and the high discharge potential can be obtained for single-metal doped α-$Ni(OH)_2$, the performance of Ni-MH batteries can be partially worse, such an capacity fading, high internal resistance and short cycle life at high charge–discharge rates [8]. Besides, the oxygen evolution becomes easier and the difference between oxygen evolution potential and oxidation potential becomes smaller after adding single metal ion. These are unfavourable to improve the electrochemical activity of batteries.

When the nickel hydroxide was doped by one kind of metal irons, the discharge capacity is generally decreased with the increase of scan rate or charge–discharge current. Liu and Anderson [9] pointed out that this phenomenon was caused by the undeveloped diffuse-layer of active materials in porous electrodes, because the discharge capacity of batteries is dominated by both the diffusive resistance and the proton diffusion in host materials. Watannabe and Kikuoka [10] reported that nickel hydroxide with a smaller crystalline size showed better charge–discharge cyclic characteristic and a higher proton diffusion coefficient. Moreover, many groups have investigated the relationship between structure defects and electrochemical reactivity of nickel hydroxide and concluded that both the structural defects and the disorder of nickel hydroxide can improve their properties [11–13]. In order to enhance characteristics of nickel hydroxide, numerous studies have been carried out through the substitution with two elements, such as Al–Co [14], Al–Y [15], Co–Zn [16]. Although the electrochemical performance has been further improved, the results are still not satisfying because of powder agglomeration, serious oxygen evolution reaction, and diffusion barrier. Based on the above consideration, in the present study, we have synthesized multi-element doped α-nickel hydroxides by supersonic co-precipitation method, which has an ideal disordered structure, and the effect of multi-element additives on structure and electrochemical performance has been studied in details.

2. Experimental

2.1. Preparation of nickel hydroxide with different additives

The multi-element doped α-nickel hydroxides were prepared by a supersonic co-precipitation method at 50 °C. A mixed solution containing $NiCl_2{\cdot}6H_2O$, $Al_2(SO_4)_3{\cdot}18H_2O$, $Co(NO_3)_2$ $6H_2O$, $YCl_3{\cdot}6H_2O$, $ZnSO_4$ $18H_2O$ (the molar ratio of Ni:Al:Co:Y:Zn is 1:0.12:0.20:0.05:0.05) and a proper amount of sodium hydroxide aqueous solution were dropping into a mother liquid synchronously under agitation. Sodium hydroxide was modulated to keep the pH value at 9.00 ± 0.10 by pH meter. The agitation lasted 5 h after dropping was finished, and supersonic was

* Corresponding author. Tel.: +86 02039322265; fax: +86 02039322265.
E-mail address: yanjuanzhu007@126.com (Y.J. Zhu).

0925-8388/$ – see front matter © 2011 Elsevier B.V. All rights reserved.
doi:10.1016/j.jallcom.2011.03.104

Table 1
The substituted composition and particle size of samples.

Samples	Nominal composition	Particle size (nm)
A	$Ni_{75.7}Al_{9.1}Co_{15.2}$	62
B	$Ni_{73.1}Al_{8.7}Co_{14.6}Y_{3.6}$	56
C	$Ni_{70.5}Al_{8.4}Co_{14.1}Y_{3.5}Zn_{3.5}$	49

applied in all above processes. The suspension was aged for 12 h at 50 °C, and then washed three times with distilled water and twice with anhydrous ethanol. Finally, the attained nickel hydroxide product was filtered and dried to constant weight at 80 °C (sample C obtained). The similar procedure was carried out to synthesize sample A (Ni:Al:Co = 1:0.12:0.20) and sample B (Ni:Al:Co:Y = 1:0.12:0.20:0.05).

2.2. Preparation of nickel hydroxide electrodes

The pasted nickel electrodes were prepared as follows: 8 wt.% samples A, B or C, 86 wt.% commercial micro-size spherical nickel, 3 wt.% nickel powder, and 2 wt.% CMC were mixed thoroughly with 1 wt.% PTFE solution. The paste obtained was incorporated into nickel foam substrates with the geometrical size of 2.5 cm × 2.5 cm. The pasted electrodes were dried naturally and then mechanically pressed.

2.3. Physical characterization

The crystal structure was determined by X-ray diffraction (XRD) using a D/Max-IIIA X-ray diffractometer with CuKα radiation (λ = 1.54 Å) at 36 kV and 20 mA. Particle size distribution (PSD) was carried out using a Nanotrac 150 particle size analyzer.

2.4. Electrochemical measurements

All electrochemical studies were performed in a three-compartment electrolysis cell at ambient temperature. The test cell is comprised of a working electrode (the positive electrode), a counter electrode (made of AB_5 type hydride alloy), and an Hg/HgO reference electrode. Electrolyte with 7 M KOH and 0.05 M LiOH was used. Both cyclic voltammetry (CV) and electrochemical impedance measurements(EIS) were carried out using a Chenhua CHI7600 model Electrochemical Workstation. The scan rate of CV test ranges from 0.02 V/s to 0.10 V/s and the cell potential ranges from −0.2 V to 0.7 V. EIS measurements were made at open circuit potential in the frequency range of 10 kHz to 1 Hz.

Simulated batteries are assembled by using the prepared nickel hydroxide electrode as anode, a hydrogen storage alloy electrode as the cathode, and polypropylene as the separator between the anode and cathode. Galvanostatic charge/discharge test was carried out at 0.1 C and 0.5 C rate using a Neware BTS-51800 battery testing system. The electrodes were discharged to 1.0 V at ambient temperature.

3. Results and discussion

3.1. Characterization of nickel hydroxide samples

The nominal compositions and average particle size of samples A, B, C are presented in Table 1. The particle size distributions (PSD) are shown in Fig. 1. It can be seen that the average diameters of samples A and B are almost the same from Table 1, but much bigger than that of sample C. Fig. 1 shows that three samples have narrow

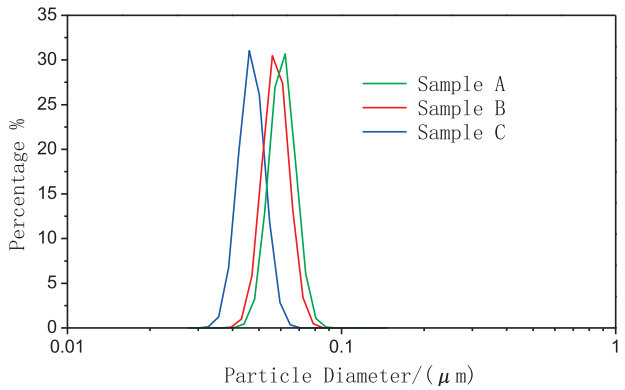

Fig. 1. Particle size distribution for samples A, B, C.

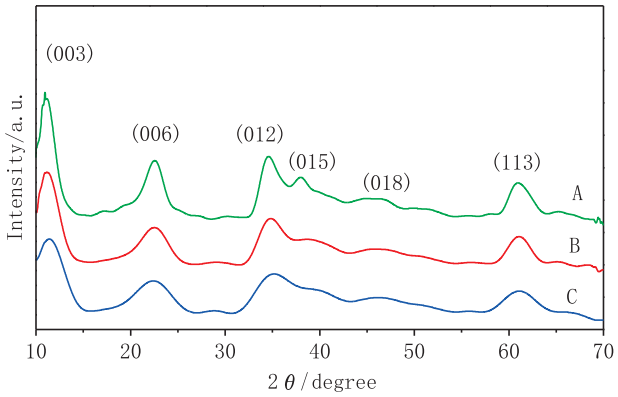

Fig. 2. XRD patterns of samples A, B, C.

particle size distribution, indicating that the size of three samples is uniform. The particle size distribution of these samples ranges 34–91 nm. The result is larger than the value (20–60 nm) calculated from XRD, which may be due to uneven grind.

The XRD patterns of α-nickel hydroxides samples A–C are presented in Fig. 2. The peak position for each sample is well matched with that of the standard substance α-$Ni(OH)_2{\cdot}0.75H_2O$ (ICDD-JCPDS 38-0715). The asymmetrical diffraction peak located in the range of 32–36° is the characteristic of the turbostratic disorder in α-nickel hydroxide [17]. The full width of the half maximums (FWHMs) of the respective sample in all reflections tend to increase in a sequence of A, B, C, which indicates the decreasing crystallite size, and is in accordance with the results in Fig. 1. This result is probably caused by an increase in the amount of crystalline defects in the $Ni(OH)_2$ lattice with increase of additives. Moreover, the peak intensity of all samples reduces with increase of additives, which indicates a decrease of the crystallinity in the samples. A low crystallization degree material means a higher electrochemical performance of nickel-based batteries, according to Liu and Li [18]. Thus, sample C can be expected to have a better electrochemical performance than that the others.

3.2. Cyclic voltammetric behavior

Cyclic voltammograms of samples A, B, C at a scanning rate of 0.10 V/s are plotted in Fig. 3. The cyclic voltammetric parameters corresponding to Fig. 3 are tabulated in Table 2. The ΔE_{OR} is taken as an estimate of the reversibility of the redox reaction, the smaller is ΔE_{OR}, the more reversible is the electrochemical reaction [19]. The sample C has smaller ΔE_{OR} than the others, and thus has better electrochemical reversibility in charge–discharge process. The oxygen evolution reaction (OER) is known as a parasitic reaction during the charge process, which limits the electrochemical performance of nickel hydroxide electrodes. To compare the effect of multi-element doping on the oxygen evolution reaction, the sepa-

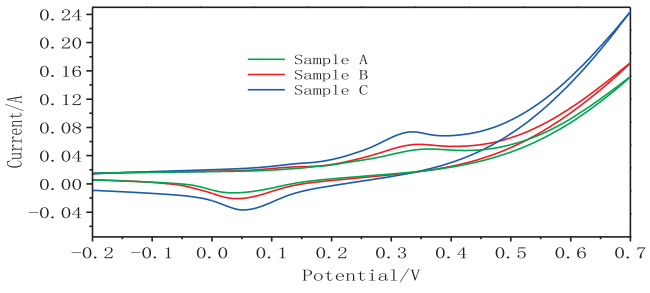

Fig. 3. CV curves of samples A, B, C at a scanning rate of 0.10 V/s.

Table 2
Results of cyclic voltammetry measurements.

Samples	E_O (V)	E_R (V)	E_{OER} (V)	ΔE_{OR} (V)	$E_{OER} - E_O$ (V)
A	0.364	0.036	0.436	0.328	0.072
B	0.347	0.042	0.424	0.305	0.077
C	0.335	0.053	0.412	0.282	0.087

E_O, the oxidation peak potential; E_R, the reduction peak potential; E_{OER}, the oxygen evolution potential; ΔE_{OR}, the difference between the reduction peak potential and the oxidation peak potential.

ration between the oxidation peak potential and the OER potential ($E_{OER} - E_{OR}$) is estimated from the voltammograms. According to the data in Table 2, the sequence of the ($E_{OER} - E_{OR}$) value is sample C > sample B > sample A. The highest $E_{OER} - E_{OR}$ value obtained for sample C clearly demonstrates all the doped elements in nickel hydroxide may produce the synergic effect and enhance the performance of the active material effectively [20]. In addition, due to the increase in the $E_{OER} - E_{OR}$ separation of nickel hydroxide, the charge efficiency of the electrodes can be markedly improved, which indicates that the sample C electrode has the greatest discharge capacity, as reported in Ref. [21].

In case of semi-infinite diffusion, the peak current I_p may be expressed by the classical Randle-Sevick equation [22]:

$$I_p = (2.69 \times 10^5) \times S \times n^{3/2}(D\upsilon)^{1/2}C^0 \quad (1)$$

where I_p is anodic peak current; n is the electronic number of reaction(the value is about 1 for nickel hydroxide); S is the real surface area of the electrode, D is the diffusion coefficient; υ is the scan rate; C^0 is the initial concentration of active material.

Fig. 4 shows the cyclic voltammograms of samples A, B, C at various scanning rates. As the scan rate increases, the anodic peak potential shifts to a more positive direction, while the cathodic peak only has a slight movement towards the negative direction. A linear relationship between oxidation peak current I_p and square root of scanning rate $\upsilon^{1/2}$ can be found in Fig. 5, indicating that all samples are controlled by proton diffusion. From the linear slope in Fig. 5 and Eq. (1), it can be calculated that the proton diffusion coefficients in samples A, B, C is 3.94×10^{-9}, 6.59×10^{-9},1.75×10^{-8} cm^2/s, respectively. The result shows that the Al/Co-Y-Zn codoped

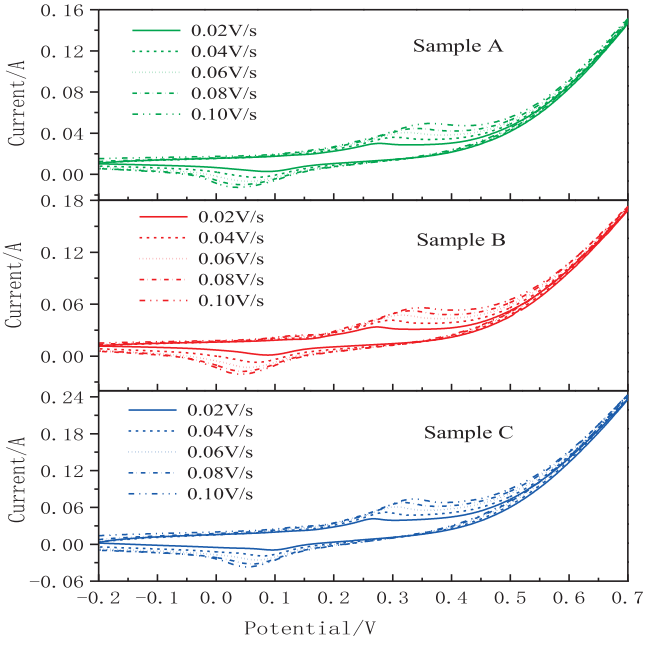

Fig. 4. Cyclic voltammograms of samples A, B, C at various scan rates.

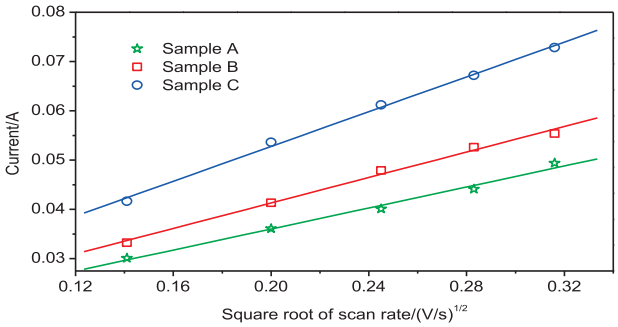

Fig. 5. Relationship between the anodic peak current and the square root of scan rate for samples A, B, C.

α-nickel hydroxide has the largest proton diffusion coefficient, this is probably due to the more crystal defects formed in the nickel hydroxide host lattice (discussed in Section 3.1), which provide better path for diffusion of protons within the NiO lays [23]. Moreover, the stacking faults and growth defects can produce vacancies for enhanced proton conduction in the host lattice. Conversion between α/γ couple is accelerated during the charge–discharge process, which results in increasing discharge capacity for nickel hydroxides [3,24].

3.3. Electrochemical impedance spectroscopy measurement

Fig. 6 presents EIS of samples A, B, C at steady state. The semicircle at high frequencies (HF) is the characteristic of the charge-transfer resistance (R_t) acting in parallel with the double layer capacitance [25]. At low frequencies (LF), three straight lines having an angle of 45°with the real axis indicate a linear Warburg portion, being the characteristic of the semi-infinite diffusion. Fig. 6 shows that the resistance of the solution (R_L) of three electrodes are almost the same, while there is a large difference in R_t with $R_{t,C} < R_{t,B} < R_{t,A}$ (the larger the diameter of the semicircle, the larger R_t) [26]. This result implies that electrochemical polarization decreases with the increase of additives. The electrochemical polarization is correlated with the discharge potential (the smaller polarization, the larger discharge potential) [27]. Thus, the results of EIS suggest that the discharge potential of samples A, B, C is as follows: C > B > A.

The explanations to above results are presented as follows: more anions (Cl^-, NO_3^-, etc.) can be intercalated to the interlayer of nickel hydroxide in order to keep charge neutrality with increase of additives. It is known that H^+ and OH^- run the fastest in aqueous solution because there is a relay system [28], which usually takes action in the process of oxidation or reduction. The increase of additives makes more space for water molecules, which strengthens the relay system of the transportation of H^+ [29]. Therefore, the proton

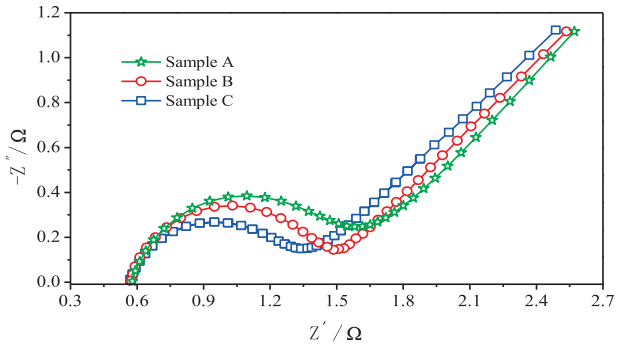

Fig. 6. Electrochemical impedance spectroscopy of samples A, B, C.

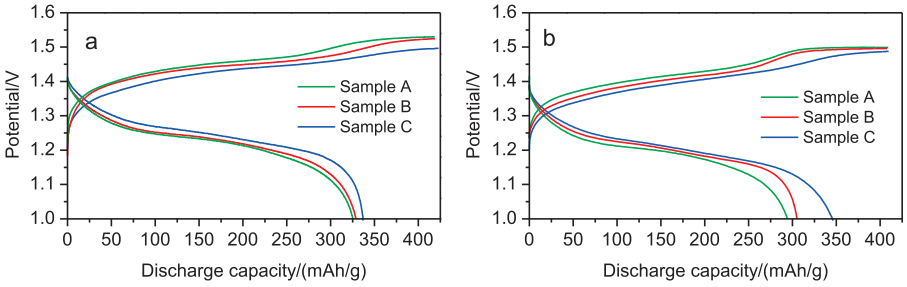

Fig. 7. Charge–discharge curves of samples A, B, C at (a) 0.1 C and (b) 0.5 C charge–discharge rates.

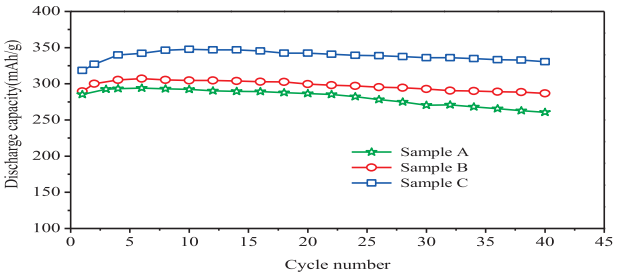

Fig. 8. Cyclic performance of samples A, B, C at 0.5 C discharge rate.

diffusion is enhanced greatly and the charge-transfer resistance is decreased with increase in the amount of additives.

3.4. Galvanostatic charge–discharge measurement

Fig. 7 is the charge–discharge curves of the three nickel electrodes at 0.1 C and 0.5 C rate, respectively. It can be seen from Fig. 7(a) that the discharge capacities of samples A, B, C are slight different at 0.1 C rate, which is 326, 330 and 337 mAh/g, respectively. It indicates that at low charge–discharge rate (less than 0.2 C) influences the discharge capacity very little. At 0.5 C rate, the discharge capacities of samples B and C reach 305 and 346 mAh/g, which are much higher than that (294 mAh/g) of sample A, as shown in Fig. 7(b). However, it is unusual that the discharge capacity (346 mAh/g) of sample C is even larger at 0.5 C rate than that (337 mAh/g) at 0.1 C rate, while the discharge capacities at 0.5 C rate are much lower than that at 0.1 C rate for samples A and B. The result indicates the oxygen evolution reaction can be efficiently restrained in sample C and the charge efficiency at high discharge rate is improved. Moreover, the sample C has a lower charge potential and higher discharge potential compared with samples A and B, which is in good agreement with the CV and EIS tests.

The cyclic performance of three samples at 0.5 C rate is shown in Fig. 8. It cam be seen that three curves show the similar shape that discharge capacity increases firstly, then reduces after reaching the maximum value. In order to quantitatively characterize the cyclic stability, the deterioration rate (R_d) [30] is used. The R_d for samples A, B, C is 11.3%, 5.8%, 3.7%, respectively. It indicates that the sample C has higher discharge capacity and better cycling stability than that of samples A and B. The excellent cyclic performance for sample C is brought by the ideal disordered structure and faster diffusion kinetics in α phase nickel hydroxide.

4. Conclusions

The α-nickel hydroxides substituted with several elements have been prepared by supersonic co-precipitation method. The dopants were found to be the key factor that affected the crystal structure and electrochemical behavior. The XRD results show that the synthesized samples possessed a reduced particle size and increased crystalline defects with increase of doped elements. The cyclic voltammetry (CV) and electrochemical impedance spectroscopy (EIS) show sample C has the best reaction reversibility and highest proton diffusion coefficient. The charge–discharge tests show that the 0.5 C discharge capacity (346 mAh/g) of sample C is larger than that (337 mAh/g) at 0.1 C rate, while the discharge capacity at 0.5 C rate is much lower than that at 0.1 C rate for samples A and B. These results suggest that multi-elements are effective in improving the electrochemical activity of nickel hydroxide electrodes.

Acknowledgements

This work was supported by the National Natural Science Foundation of China (No. 10774030), and by the Science and Technology Program of Guangzhou City of China (No. 2008J1-C161).

References

[1] R.S. Jayashree, Vishnu, P. Kamath, J. Power Sources 107 (2002) 120.
[2] B. Liu, H.T. Yuan, Y.S. Zhang, Int. J. Hydrogen Energy 29 (2004) 453.
[3] L. Indrin, M. Dixit, P.V. Kamath, J. Power Sources 52 (1994) 93.
[4] Y.L. Zhao, J.M. Wang, H. Chen, T. Pan, J.Q. Zhang, C.N. Cao, Int. J. Hydrogen Energy 29 (2004) 889.
[5] C.Y. Wang, S. Zhong, D.H. Bradhurst, H.K. Liu, S.X. Dou, J. Alloys Compd. 330 (2002) 802.
[6] L. Demourgues-Grerlou, L. Fournes, J. Power Sources 45 (1993) 281.
[7] C. Tessier, L. Demourgues-Grerlou, C. Faure, Solid State Ion 133 (2000) 11.
[8] G.A. Snook, N.W. Duffy, A.G. Pandolfo, J. Power Sources 168 (2007) 513.
[9] K.C. Liu, M.A. Anderson, J. Electrochem. Soc. 143 (1996) 124.
[10] K. Watannabe, T. Kikuoka, J. Appl. Electrochem. 25 (1995) 219.
[11] M.C. Bernard, R. Cortes, M. Keddam, H. Takenouti, P. Bernard, S. Senyarich, J. Power Sources 63 (1996) 247.
[12] R.S. Jayashree, P.V. Kamath, G.N. Subbanna, J. Electrochem. Soc. 147 (2000) 2029.
[13] T.N. Ramesh, P.V. Kamath, J. Electrochem. Soc. 152 (2005) A806.
[14] E. Scavetta, M. Berrettoni, F. Nobili, D. Tonelli, Electrochim. Acta 50 (2005) 3305.
[15] C.J. Liu, H.B. Wu, Y.W. Li, J. Phys. Chem. Solids 70 (2009) 723.
[16] X. Mi, X.P. Gao, C.Y. Jiang, M.M. Geng, J. Yan, C.R. Wan, Electrochim. Acta 49 (2004) 3361.
[17] D.N. Yang, R.M. Wang, M.S. He, J. Zhang, Z.F. Liu, J. Phys. Chem. 109 (2005) 7654.
[18] C.J. Liu, Y.W. Li, J. Alloys Compd. 478 (2009) 415.
[19] Q.S. Song, C.H. Chiu, S.L.I. Chan, J. Appl. Electrochem. 6 (2006) 97.
[20] W.G. Zhang, W.Q. Jiang, L.M. Yu, Z.Z. Fu, W. Xia, M.L. Yang, Int. J. Hydrogen Energy 34 (2009) 473.
[21] D.A. Corrigan, R.M. Bendert, J. Electrochem. Soc. 136 (1989) 12.
[22] D.M. Mac Arthur, J. Electrochem. Soc. 117 (1970) 422.
[23] T.N. Ramesh, P.V. Kamath, Mater. Res. Bull. 43 (2008) 2827.
[24] X.J. Han, P. Xu, C.Q. Xu, L. Zhao, Z.B. Mo, T. Liu, Electrochim. Acta 50 (2005) 2763.
[25] J. Musilova, J. Jindra, P. Mrha, J. Novak, K. Garche, Wiesener, J. Power Sources 21 (1987) 67.
[26] S.A. Cheng, J.Q. Zhang, M.H. Zhao, C.A. Cao, J. Alloys Compd. 293 (1999) 814.
[27] Y.L. Zhao, J.M. Wang, H. Chen, T. Pan, J.Q. Zhang, C.N. Cao, Electrochim. Acta 50 (2004) 91.
[28] P. Atkins, J.D. Paula, Physical Chemistry, 7th ed., Oxford University Press, Oxford, 2002.
[29] Y.W. Li, J.H. Yao, C.J. Liu, W.M. Zhao, W.X. Deng, S.K. Zhong, Int. J. Hydrogen Energy 35 (2010) 2539.
[30] H. Chen, J.M. Wang, T. Pan, J.Q. Zhang, C.N. Cao, Int. J. Hydrogen Energy 27 (2002) 489.